AGU PUBLICATIONS

JGR

Journal of Geophysical Research: Oceans

RESEARCH ARTICLE

10.1002/2013JC009470

Key Points:
- Anticyclonic eddy carried low oxygen water from the Chilean shelf to ~20°S, 85.5°W
- Water mass in the eddy was isolated for about 11 months
- Sea surface height anomaly is not sufficient to specify eddy strength

Correspondence to:
L. Stramma,
lstramma@geomar.de

Citation:
Stramma, L., R. A. Weller, R. Czeschel, and S. Bigorre (2014), Eddies and an extreme water mass anomaly observed in the eastern south Pacific at the Stratus mooring, *J. Geophys. Res. Oceans*, *119*, 1068–1083, doi:10.1002/2013JC009470.

Received 27 SEP 2013
Accepted 26 JAN 2014
Accepted article online 31 JAN 2014
Published online 12 FEB 2014

Eddies and an extreme water mass anomaly observed in the eastern south Pacific at the Stratus mooring

Lothar Stramma[1], Robert A. Weller[2], Rena Czeschel[1], and Sebastien Bigorre[2]

[1]Helmholtz Centre for Ocean Research Kiel (GEOMAR), Kiel, Germany, [2]Department of Physical Oceanography, Woods Hole Oceanographic Institution, Woods Hole, Massachusetts, USA

Abstract In the tropical eastern South Pacific the Stratus Ocean Reference Station (ORS) (~20°S, 85.5°W) is located in the transition zone between the oxygen minimum zone (OMZ) and the well-oxygenated subtropical gyre. In February/March 2012, extremely anomalous water mass properties were observed in the thermocline at the Stratus ORS. The available eddy oxygen anomaly was -10.5×10^{16} µmol. This anomalous water was contained in an anticyclonic mode-water eddy crossing the mooring site. This eddy was absorbed at that time by an anticyclonic feature located south of the Stratus mooring. This was the largest water property anomaly observed at the mooring during the 13.5 month deployment period. The sea surface height anomaly (SSHA) of the strong mode-water eddy in February/March 2012 was weak, and while the lowest and highest SSHA were related to weak eddies, SSHA is found not to be sufficient to specify the eddy strength for subsurface-intensified eddies. Still, the anticyclonic eddy, and its related water mass characteristics, could be tracked backward in time in SSHA satellite data to a formation region in April 2011 off the Chilean coast. The resulting mean westward propagation velocity was 5.5 cm s^{-1}. This extremely long-lived eddy carried the water characteristics from the near-coastal Chilean water to the open ocean. The water mass stayed isolated during the 11 month travel time due to high rotational speed of about 20 cm s^{-1} leading to almost zero oxygen in the subsurface layer of the anticyclonic mode-water eddy with indications of high primary production just below the mixed layer.

1. Introduction

We focus here on the eastern South Pacific off northern Chile and on observations collected from a mooring close to 20°S, 85.5°W, some 1500 km offshore. The eastern boundary region of the South Pacific draws interest from a number of perspectives. The coastal upwelling associated with the Trade Winds gives rise to a productive and economically important ecosystem. This coastal region is characterized by cool sea surface temperatures (SST) and by persistent low cloud cover [e.g., *Colbo and Weller*, 2007; *Mechoso et al*., 2014]. Off northern Chile, the surface layer of the ocean is relatively warm (Figure 1a) and salty, and evaporation dominates precipitation [e.g., *Colbo and Weller*, 2007; *Mechoso et al*., 2014]. In the ocean, below the surface layer of the South Pacific Eastern Subtropical Surface Water, there is a cool, fresh water layer [Subtropical Underwater, *Fiedler and Talley*, 2006] and then below is a subsurface layer (South Pacific Eastern Subtropical Mode Water) with particularly low oxygen concentration that also extends offshore at depths of 100–900 m.

The desire to understand and accurately model the physical and biogeochemical dynamics of this region has motivated a number of studies. Targets of the VOCALS program (VAMOS Ocean Cloud Atmosphere Land Study, part of the Variability of the American Monsoon Systems component of CLIVAR, the Climate Variability and Predictability research program of the World Climate Research Programme) and its collaborative field campaign in the region at around 20°S were improved understanding of the processes that both control SST and the amount and type of cloud in the region [*Mechoso et al*., 2014]. In the oceanographic components of this campaign, there was a particular focus on the role of eddies. Some work suggested that westward propagating eddies play a role in cooling and freshening the warm, salty surface mixed layer [*Colbo and Weller*, 2007]. *Colas et al*. [2012] concluded the eddy contribution to the heat balance was substantial, with cyclonic eddies influencing the surface layer and anticyclonic eddies influencing the subsurface. Eddy buoyancy fluxes are shoreward and upward in the upper ocean and serve to balance mean offshore air-sea heating and coastal upwelling [*Colas et al*., 2013]. Work by *Holte et al*. [2013], however, stated that eddies are not as important to the upper-ocean heat budget as *Colbo and Weller* [2007] suggested. Still, work continues on the roles that eddies play in the region, including the possibility that eddies

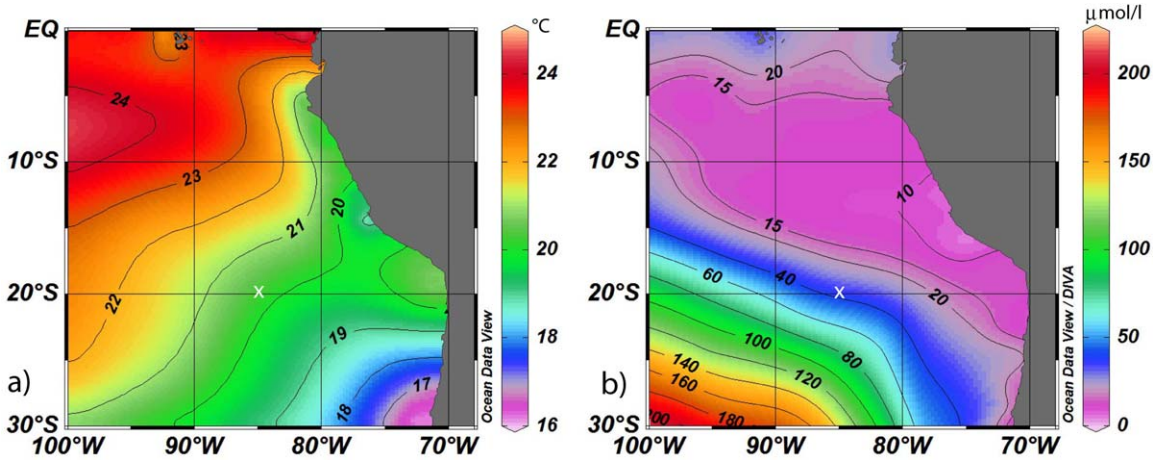

Figure 1. Maps of the mean climatological distribution using the World Ocean Database 2009 [e.g., *Boyer et al*., 2009] for (a) sea surface temperature in °C and (b) oxygen in µmol L^{-1} at the density surface $\sigma_\theta = 26.65$ kg m^{-3} (at about 330 m depth). The Stratus 11 site is marked with a white x.

may enhance the vertical mixing of the surface layer with the mode water below. Observations carried out in VOCALS also, for example, investigated the possibility that plankton carried westward offshore by eddies leads to increased levels of dimethylsulfide (DMS) and in turn to cloud nucleation particles that promoted the formation of the Stratus clouds [*Yang et al*., 2011].

There is also interest in considering the role of different processes in maintaining the oxygen minimum zones (OMZs) in the eastern South Pacific. Layers with particularly low oxygen concentrations, or OMZs, are located in the eastern tropical oceans at depths of 100–900 m [e.g., *Karstensen et al*., 2008]. OMZs play an essential role in the global nitrogen cycle, in which various chemical species, according to their degree of oxidation and different bacterial processes, participate [*Paulmier and Ruiz-Pino*, 2009]. OMZs are of special interest due to their influence on the ecosystem [*Bertrand et al*., 2011] and because model results [e.g., *Bopp et al*., 2002; *Matear and Hirst*, 2003] predict an increase of low oxygen layers in the future. Observations [e.g., *Stramma et al*., 2008] show decreasing oxygen over the last 50 years, especially for the tropical oceans while in the subtropical regions areas with increasing oxygen exist [*Stramma et al*., 2010b]. In the eastern tropical Pacific, eastward zonal currents [e.g., *Kessler*, 2006] could be important in resupplying oxygen to the OMZs [*Stramma et al*., 2010a]. At 400 m depth the South Equatorial Current in the northern part of the South Pacific subtropical gyre is well visible northward to about 10°S, but influenced by eddies [*Czeschel et al*., 2011]. Model results indicate that eddies are the main component in the redistribution of oxygen in the center and on the poleward side of the eastern South Pacific OMZ (N. Gruber, personal communication, 2012), leading to an eddy-induced transport of nutrients from the nearshore environment to the open ocean [*Gruber et al*., 2011].

Our understanding of oceanic mesoscale variability provides a context for considering the role of eddies. Mesoscale variability occurs as linear Rossby waves and as nonlinear vortices or eddies. In contrast to linear waves, nonlinear vortices can transport momentum, heat, mass, and the chemical constituents of seawater, and therefore contribute to the large-scale water mass distribution [e.g., *Chelton et al*., 2007]. The degree of nonlinearity of a mesoscale feature is characterized by the ratio of the rotational fluid speed U (swirl velocity) to the translation speed c of the feature. When $U/c > 1$, the feature is nonlinear, which allows it to maintain a coherent structure as it propagates [e.g., *Flierl*, 1981; *Chelton et al*., 2011a]. Two types of anticyclonic eddies exist: "regular" anticyclones in which the isopycnals in the eddy are depressed for the entire eddy extent (referred to as anticyclones in the following) and mode-water eddies in which a thick lens of water deepens the main thermocline while shoaling the seasonal thermocline [*McGillicuddy et al*., 2007]. The interaction of the eddy surface currents with the wind-driven flow generates Ekman upwelling in anticyclones and Ekman downwelling in cyclones during the formation and intensification stages. The combination of the shoaling seasonal pycnocline and the Ekman upwelling for anticyclonic mode-water eddies enhances biological activity in mode-water eddies [e.g., *Dewar and Flierl*, 1987; *Ledwell et al*., 2008]. Isopleths of

nutrients and chlorophyll-a generally lie on isopycnal surfaces. This suggests that physics is controlling the availability of nutrients to the euphotic layer and where phytoplankton can thrive [*Dickey et al*., 2008].

Mode-water eddies derive their name from the thick lens of uniform water as the term mode water identifies a water mass characterized by its vertical homogeneity [*McCartney*, 1982]. Because the geostrophic velocities are dominated by depressions of the main pycnocline, the direction of rotation in mode-water eddies is the same as in anticyclones. However, displacement of the seasonal pycnocline is upward and tends to upwell nutrients into the euphotic zone [*McGillicuddy et al*., 2007], yielding a layer of high chlorophyll concentration [*Ledwell et al*., 2008]. Early investigations of a mode-water eddy in 1981 in the California Current examined their dynamics [*Simpson et al*., 1984], surface manifestation [*Koblinsky et al*., 1984], chemical structure [*Simpson*, 1984], and plankton distribution [*Haury*, 2004]. As part of VOCALS, three anticyclonic eddies in the eastern tropical South Pacific near 20°S were studied; two featured depressed near-surface isopycnals whereas one exhibited doming isopycnals [*Holte et al*., 2013]. To the south of this region several anticyclonic subthermocline eddies with a subsurface radial velocity maximum have also been described [*Johnson and McTaggart*, 2010].

Using 15 years of satellite altimetry, an analysis of the mean eddy properties offshore the Peruvian coast found many eddies in this region, most frequently off Chimbote (9°S) and south of San Juan (15°S) [*Chaigneau et al*., 2008]. The most eddies were seen between 15°S and 18°S, east of 90°W. From a survey in November 2012 the parameter distribution of nutrients in three particular eddies off southern Peru at ~16°45′S was described [*Stramma et al*., 2013]. A similar survey exists for near-shelf eddies off central-southern Chile [*Morales et al*., 2012]. Using a combination of Argo float profiles and satellite data the three-dimensional mean eddy structure of the eastern South Pacific was described for the temperature, salinity, density, and geostrophic velocity field of cyclonic as well as anticyclonic eddies [*Chaigneau et al*., 2011]. Cyclonic eddies are strongest at about 150 m depth while the core of anticyclonic eddies is located at ~400 m depth within the 26.0–26.8 kg m^{-3} density layer; these anticyclonic eddies are likely to be shed by the subsurface poleward Peru-Chile Undercurrent [*Johnson and McTaggart*, 2010; *Chaigneau et al*., 2011]. In the North Pacific at the Hawaii Ocean Time-series site (HOTS, ~23°N, 158°W) extremely anomalous water mass properties were observed in January 2001, consistent with a submesoscale vortex, possibly a remnant of a mesoscale eddy [*Lukas and Santiago-Mandujano*, 2001].

In this study, we make use of time series collected from a mooring deployed at about 20°S, 85.5°W known as the Stratus Ocean Reference Station (ORS). The Stratus ORS is located south of the OMZ (Figure 1b) at the northern end of the subtropical gyre. A hydrographic section along 88°W taken in 1993 provides spatial context for discussion of the eastern South Pacific near the Stratus mooring. From this section, a thick layer of extremely low oxygen content centered roughly at $\sigma_\theta = 26.6$–27.0 kg m^{-3} was found with particularly low oxygen content north of the location of the Stratus ORS, between 3°S and 17.5°S [*Tsuchiya and Talley*, 1998]. The climatological eddy frequency at the Stratus location is about 25% and low compared to the regions closer to southern Peru with eddy frequencies of up to 50% with the number of cyclonic and anticyclonic eddies about the same and with amplitudes in sea surface height of up to 5 cm [*Chaigneau et al*., 2008]. As the eddies predominantly move westward with small poleward displacements for cyclonic and equatorward components for anticyclonic eddies [*Chaigneau et al*., 2008], the formation region of eddies observed at the Stratus ORS will be preferentially off northern Chile.

Here we use a recent, comprehensive Stratus ORS data set that includes observations of dissolved oxygen as well as of temperature, salinity, and velocity together with altimeter sea surface height anomaly (SSHA) data to describe eddies in the region, focusing on those observed by the Stratus ORS. In particular, we describe a strong anticyclonic eddy observed at the Stratus ORS, the path of that eddy, and the anomalous water carried westward by that eddy. This contributes to a better understanding of the redistribution of water masses in the OMZ and the role of eddies in that redistribution.

2. Data

Since October 2000, the Stratus ORS has been maintained at about 20°S, 85.5°W to collect an accurate record of surface meteorology and air-sea fluxes of heat, freshwater, and momentum [*Colbo and Weller*, 2009], to examine the variability of sea-surface temperature, and to observe the temporal evolution of the vertical structure of the upper ocean [*Colbo and Weller*, 2007]. For more specific details on the mooring and

Table 1. Distribution of the Oxygen Optodes and Other Sensors Deployed on the Stratus 11 Mooring for the Period 6 April 2011 to 29 May 2012

Depth (m)	Instrument	Oxygen	Velocity	Other Parameter
10	Nortek		yes	
13	RCM 11		yes	
16	Microcat		no	T (SBE 37)
20	RCM 11		yes	
25	SBE 39		no	T
32.5	RCM 11		yes	
35	SBE 39		no	T
45	SeaGuard	Optode	yes	T (SBE 39) 1.5 m below (O_2 stopped 12 Apr 2012)
62.5	Microcat		no	T (SBE 37)
87.3	SeaGuard	Optode	yes	(O_2 stopped 26 Jan 2012)
135	Workhorse		yes	(stopped 30 Dec 2011)
145	SeaGuard	Optode	yes	(O_2 stopped 5 Apr 2012)
160	Microcat		no	T,S (SBE 37)
235	SeaGuard	Optode	yes	T (SBE 39) 1.5 m below
290	SeaGuard	Optode	yes	T,S (Microcat) 5 m below
320	VMCM		yes	T (stopped 17 Apr 2012)
322	Oxygen-logger	Optode	no	
349	VMCM		yes	T
353	Oxygen-logger	Optode	no	
400	SeaGuard	Optode	yes	T,S (Microcat) 1 m below
450	SeaGuard	Optode	yes	T,S (Microcat) 1 m below
601	SeaGuard	Optode	yes	T,S (Microcat) 1 m below
803	VMCM		yes	T (stopped 30 Nov 2011)

instrumentation, including preparation, deployment, recovery, and data processing, see Appendix A. The data set we are discussing here comes from the 11th deployment of the Stratus mooring, the first in which oxygen sensors were deployed. The eleventh mooring (Stratus 11) was deployed on 6 April 2011 on *RV* Moana Wave at 19°41′S, 85°34′W and was recovered on 29 May 2012 on *RV* Melville. Ten oxygen sensors were deployed to observe the oxygen field in the upper ocean. As on earlier deployments velocity, temperature, and salinity were recorded and the combined data set (Table 1) was used.

In April 2011, eight floats with Aanderaa oxygen sensors were deployed at about 20°S east of 85°W. One of these floats (float WMO 6900873) with a parking depth at 1000 m and profiling every 10 days was located in the anticyclonic mode-water eddy described here between 12 July and 30 October 2011 and will be used to investigate the subsurface distribution when in the eddy. Unfortunately due to a float programming error in the oxygen recording software (the highest values of the B-phase were not resolved) the lowest oxygen values could not be recorded, and the oxygen record has to be taken from a deeper layer with slightly higher oxygen values.

Aviso satellite derived SSHA data were obtained and used to document the path of the strong anticyclonic eddy. Most SSHA data used in this study are delayed time products and combine all available satellite data. The weekly data are resampled on a 0.25° × 0.25° grid, projected on the mean day of the 7 day period; they are calculated with respect to a 7 year mean. In addition, near real-time daily data were used to examine the SSHA at the Stratus location (http://www.aviso.oceanobs.com). To facilitate eddy identification, the Aviso SSHA fields were spatially high-pass filtered in two dimensions to remove variability with wavelengths larger than 20° of longitude by 10° of latitude [*Chelton et al.*, 2011b]. The mean climatological parameter distributions were derived with ocean data view using the World Ocean Atlas 2009 [e.g., *Boyer et al.*, 2009].

3. Eddy Observations

3.1. Stratus Mooring Observations

For the Stratus 11 deployment, the SSHA at the mooring shows enhanced high-pass filtered SSHA from October to December 2011 with a maximum of 7 cm in early November 2011 and another relative high SSHA in February and March 2012 with 1 cm followed by the lowest SSHA of −9.5 cm in April 2012 (Figure

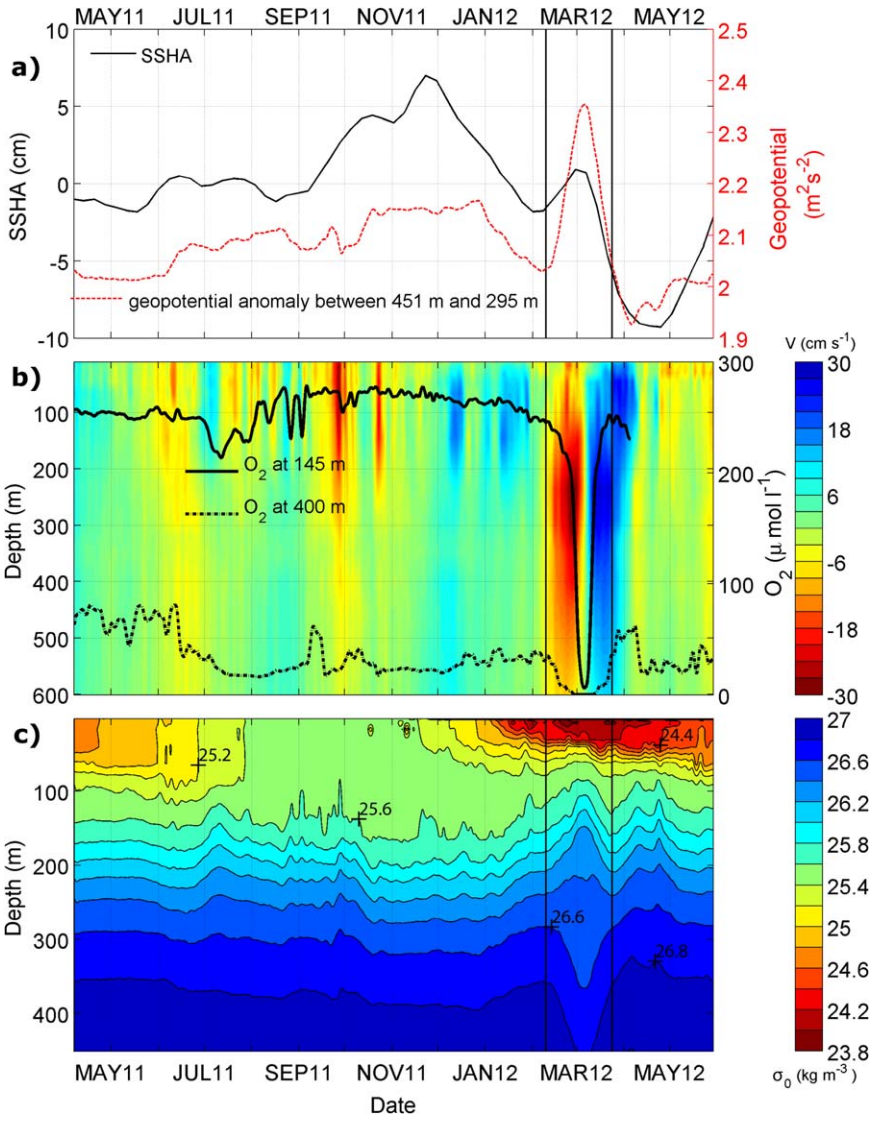

Figure 2. Time series at Stratus 11 between 6 April 2011 and 29 May 2012 for (a) weekly delayed, high-pass filtered sea surface height anomaly (in cm; black curve) and geopotential anomaly between 451 and 295 m depth in $m^2\ s^{-2}$; dashed red curve, (b) meridional velocity in cm s^{-1} (color) in the upper 600 m, with 90 h low-pass filtered oxygen time series at 145 m (solid gray line; ending 5 April 2012 due to sensor problems) and 400 m (thick black line; oxygen label on the right), and (c) density distribution in kg m^{-3} for the upper 450 m depth, from 90 h low-pass filtered hourly averaged data. Density contour interval is 0.2 kg m^3. The dates bounding the passage of the strong anticyclone are marked by vertical black lines on 9 February 2012 and 24 March 2012.

2a). These SSHA extrema are related to eddies evident in the contoured velocity data (Figure 2b) and reflected in the potential density contour plot (Figure 2c). Different to the weak SSHA signal in February/March 2012, the geopotential anomaly for the subsurface layer 295–451 m shows the largest signal in February/March 2012 for the entire mooring period (Figure 2a). Although the strong northward velocity component lasts until 4 April, the passage of the strong eddy across the mooring occurred from 9 February 2012 to 24 March 2012. The start on 9 February is marked by the onset of strong subsurface southward velocity. The end on 24 March is linked to changes in density in the upper 250 m. The northward velocity after 24 March is caused by a cyclonic eddy that follows the anticyclonic eddy. The density below 250 m returns on 24 March to a value close to that on 9 February.

The covariabilities of the moored temperature, salinity, oxygen, and density time series for two depths layers 160 and 401 m were investigated further to search for possible eddy signals (Figure 3). The SSHA anomaly in March 2012 is related to a large salinity increase of about 0.2 at 401 m depth and strong oxygen

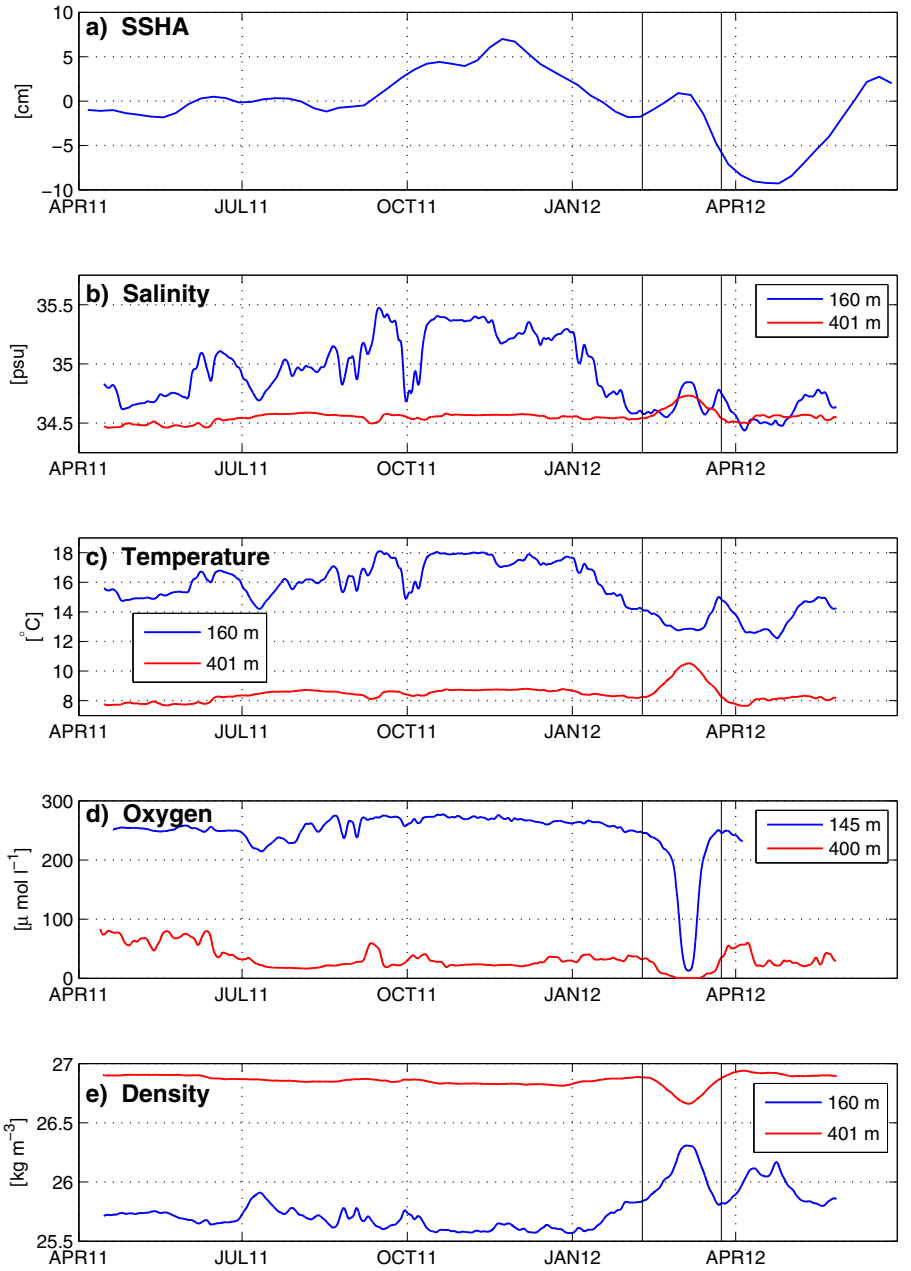

Figure 3. Time series at Stratus 11 between 6 April 2011 and 29 May 2012 of (a) weekly delayed time high-pass filtered sea surface height anomaly (in cm), and 90 h low-pass filtered, (b) salinity at 160 m (blue curve) and 401 m depth (red curve), (c) temperature (in °C) at 160 and 401 m depth, (d) oxygen (in μmol L^{-1}) at 145 and 400 m depth, and (e) density at 160 and 401 m depth. The dates for the eddy passage are marked by vertical black lines on 9 February 2012 and 24 March 2012.

decrease at 145 and 400 m depths to near zero oxygen values (Figure 3). At 145 m depth, the oxygen anomaly is larger than 200 μmol L^{-1}. The SSHA shows an anticyclonic feature at this time at the mooring, which is the only eddy-related feature during the 13.5 month deployment period with strong subsurface salinity and oxygen anomalies. The correlation coefficient for the Stratus 11 time period between temperature and salinity at 160 m and at 401 m depth within 95% confidence is 0.94 with no time shift.

The density distribution at the mooring site for the 13 month deployment period (Figure 2c) shows the unique characteristics of the anticyclonic feature in March 2012. While the density variability of other anomalies in the Stratus mooring records (Figure 2c) deviates only upward or downward, the eddy in March

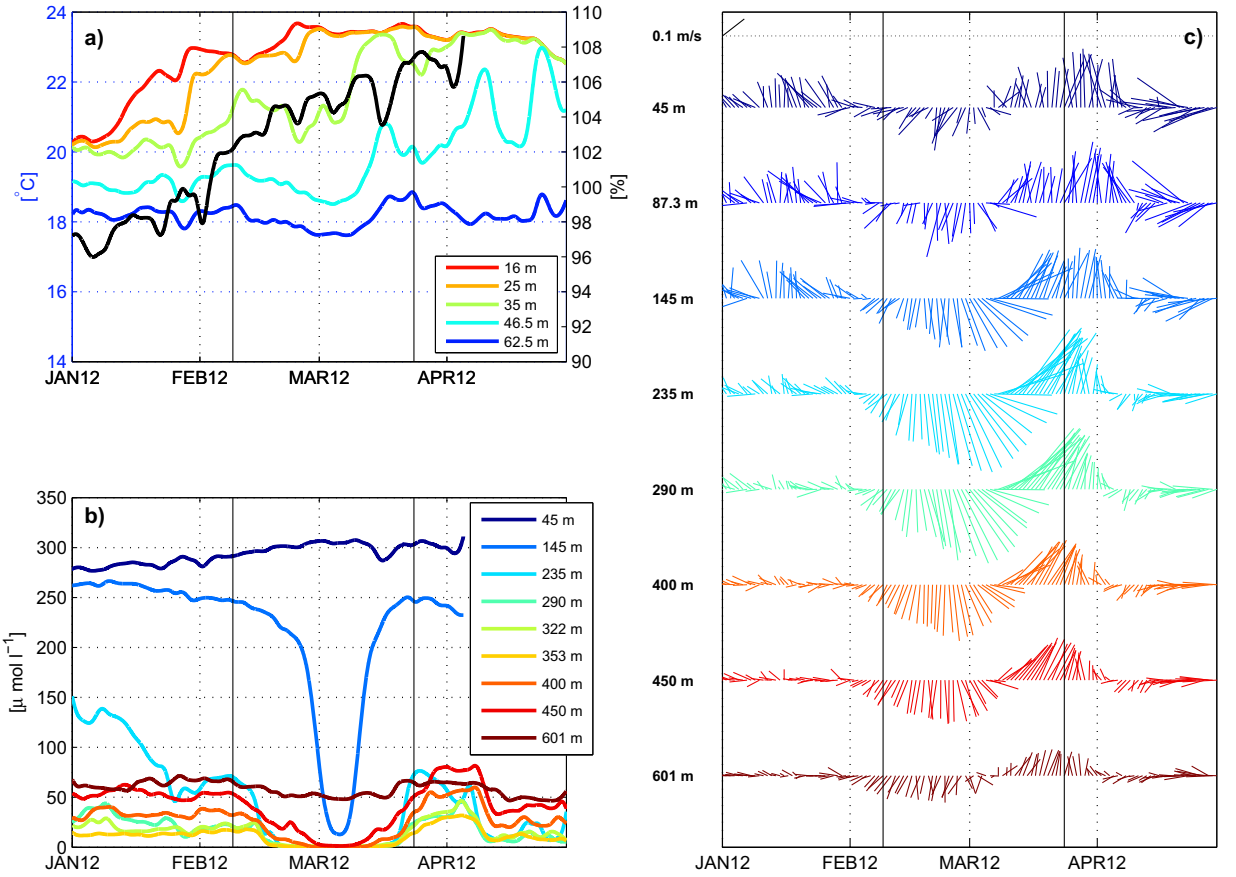

Figure 4. Time series for 1 January 2012 to 30 April 2012 at the Stratus mooring for (a) temperature (in °C) at 16, 25, 35, 46.5, and 62.5 m (see color code) and oxygen saturation (in %) at 45 m depth (black line) with a 90 h low-pass filter, (b) oxygen records (in µmol L^{-1}, color coded by depth), and (c) velocity vectors (0.1 m s^{-1} vector shown on top; color as in frame (b) measured at the Stratus mooring between 45 and 601 m depth, smoothed with a 90 h low-pass filter at the time of the passage of the anticyclonic eddy. The dates for the eddy passage are marked by vertical black lines on 9 February 2012 and 24 March 2012.

2012 shows a deepening of the isopycnals below 250 m depth and an uplift above 250 m depth, the typical distribution of a mode-water eddy.

The temperature, oxygen, and velocity time series for 1 January to 1 May 2012 at the Stratus mooring show the passage of the anticyclonic eddy from mid-February to mid-March in all records between 45 and 601 m depth (Figure 4). In the mixed layer at 45 m depth, the oxygen record shows no decrease with the lowest oxygen at about 250 µmol L^{-1} but instead an increase of oxygen up to 310 µmol L^{-1}. The related velocity vectors at 45 m as well as velocity vectors from current meters at 13, 20, and 32.5 m (not shown in Figure 4c) show the rotation of the anticyclonic eddy although weakening in the surface layer (Figure 5). All oxygen records between 145 and 450 m depth decrease to minima of between 1.25 and 0.01 µmol L^{-1} in early March 2012 for the unfiltered data (not shown) while the 145 m depth record showed high variability leading to a 90 h filtered minimum of 12.8 µmol L^{-1}. Only at 601 m depth is the decrease in oxygen weak with the lowest oxygen value of 46.7 µmol L^{-1}, the anticyclonic signal in the velocity is weak there as well.

The contour plot of meridional velocity (Figure 2b) for the entire Stratus 11 deployment period shows the unusual situation in February/March 2012. The strongest meridional subsurface velocities were connected to the anticyclone in February/March 2012. The strong southward and northward velocities cover the entire depth layer between 100 and 600 m and no similar feature was present during the entire deployment period. The superimposed oxygen records for 145 and 400 m depths show the decrease to almost zero oxygen when the core of the anticyclone passed, e.g., when the meridional velocity component changed direction. The highest swirl velocity was measured between 200 and 400 m and the swirl velocity of the anticyclone was larger than 10 cm s^{-1} between the sea surface and 600 m depth (Figure 5).

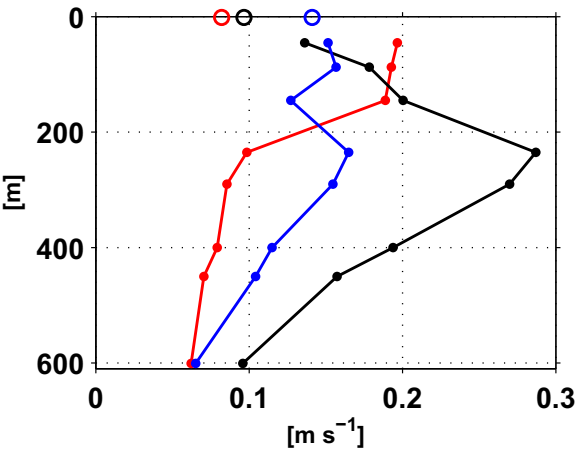

Figure 5. Swirl velocity derived from the mean of the absolute values of the strongest 90 h low-pass filtered northward and southward velocity components for September to December 2011 (red dots), 1 February to 15 March 2012 (black dots), and 16 March to 30 April 2012 (blue dots). The related meridional geostrophic surface velocities from the near real time SSHA velocity data are plotted as circles at the top.

The high SSHA from October to December 2011 at the Stratus ORS with a maximum of 7 cm is related to high salinity and temperature values at 160 m depth and slightly increased salinity and temperature values at 401 m depth, with slight covariability in oxygen. A slight decrease in oxygen at 400 m is visible (Figure 3) and the isopycnal distribution for this time period shows a small deepening between 100 and 400 m depth (Figure 2c), a typical displacement of isopycnals for an anticyclonic eddy. According to the SSHA and the velocity and density distribution at the Stratus location (Figure 2) the anticyclonic feature dominates this region from early September to the end of January. The SSHA shows a large area influenced by several anticyclonic features at this time period. The observed swirl velocities at the Stratus mooring for September to December 2011 are similar to the anticyclone in February–March 2012 in the upper 200 m (Figure 5); however, swirl velocity is low below 200 m depth. Hence, this anticyclonic feature at the end of 2011 has a small degree of nonlinearity below 200 m depth and a coherent structure was present mainly in the upper 200 m. Despite the large SSHA from October 2011 to the end of December 2011 (Figure 2) the eddy has only weak water mass characteristic anomalies.

The lowest SSHA of −9.5 cm in April 2012 is connected to low temperature and salinity at 160 and 401 m depths and high oxygen at 145 and 400 m depths (Figure 3). The density distribution shows an uplift of the isopycnals from 40 to 450 m depth (Figure 2c), the signature of a cyclonic eddy following the anticyclone which passed by in March 2012. The related northward flow is associated with the strong anticyclone. The southward flow in late April 2012 is weak compared to the swirl velocity of the anticyclone (Figure 5). Nevertheless, that southward flow is visible down to 601 m in April 2012 and increasing oxygen is observed for the records at 290 to 601 m depths (Figures 4b and 4c), associated with the weak cyclonic eddy.

3.2. Eddy Path

From altimeter data, it is possible to follow the path of the anticyclonic eddy observed in March 2012 at the Stratus mooring and thus to track the path backward in time to the formation region. On 8 February 2012, the mode-water eddy has a weak SSHA southeast of the Stratus mooring and is already connected to a larger SSHA signal to the south. On 29 February, the mode-water eddy was close to the mooring location, with the center located south of the Stratus mooring (Figure 6). The satellite data show that the surface eddy signal in SSHA disappeared at about 21 March 2012 in a strong anticyclonic feature located to the south of the Stratus mooring (Figure 6), hence the observation at the Stratus site was near the end of the lifetime of the anticyclonic eddy visible as SSHA and the path could not be followed forward in time. The anticyclonic eddy has a relatively weak signal in sea surface height anomaly figures caused by the density structure in this mode-water eddy leading to weaker surface velocities (Figure 2b). Although the locations of the eddy on the satellite maps were at times unclear, it seems certain that the anticyclonic eddy began its travel in April 2011 at the Chilean coast (Figure 7). The eddy could be tracked back to a location at 21.25°S, 72°W on 25 May 2011. Two eddies located at 19.75°S, 70.75°W and 22.5°S, 71°W on 20 April 2011 merged at the end of May 2011 at 21.25°S; 72°W, hence, two options for the origin of the eddy exist. With the lifetime of 11 months this eddy belongs to the longest-lived eddies in this region.

The mean salinity on $\sigma_\theta = 26.65$ kg m^{-3} (Figure 7a) is about 34.64 at the Stratus site and close to 34.75 near the Chilean shelf at the indicated two eddy formation locations. In the Stratus salinity record at 401 m depth in early March 2012 the salinity is about 34.75 (Figure 3). Hence, the salinity observed in the eddy in early

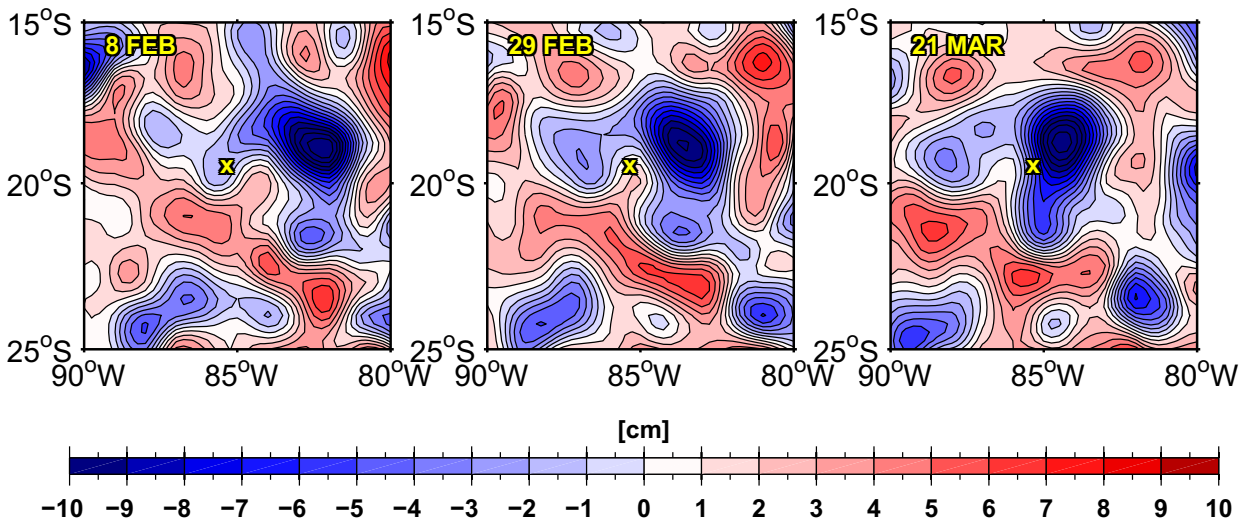

Figure 6. High-pass filtered sea surface height anomaly (in cm) near the Stratus mooring (yellow X) showing the strong anticyclonic eddy just east of the Stratus mooring north of a ridge of anticyclonic features on (left) 8 February 2012, at the Stratus mooring on (middle) 29 February 2012, and being absorbed by the anticyclonic features on (right) 21 March 2012.

March 2012 supports the satellite-based choice of a formation region on the Chilean shelf. The oxygen drops to 0.16 μmol L^{-1} in early March 2012 at the Stratus mooring in 401 m while on the mean oxygen distribution $\sigma_\theta = 26.65$ kg m^{-3} at the formation region is 10–15 μmol L^{-1} (Figures 1b and 7c), but this might be biased high due to the interpolation schemes to derive the mean field. An oxygen utilization from biogeochemistry of about 10 μM near the coast at 21°S [*Paulmier et al.*, 2006] could cause a reduction in oxygen.

The climatological mean salinity on the density σ_θ =26.9 kg m^{-3} typical for the mooring location at 401 m depth is about 34.55 and was measured before and after the passage of the anticyclonic eddy. Similarly, the oxygen at this density layer is about 40 μmol L^{-1} and hence similar to the measurements at 401 m depths before and after the passage of the eddy (Figures 4b and 4c). In addition, temperature reaches about 10.6°C at Stratus at 401 m depth in March 2012 which is similar to 10.6°C at the coast off Chile on the density $\sigma_\theta = 26.65$ kg m^{-3} (Figure 7b) while the mean temperature at the Stratus location is 8.1°C on the density $\sigma_\theta = 26.9$ kg m^{-3} in agreement with the temperatures measured at 401 m depth before and after the passage of the eddy. Hence, the observations of temperature, salinity, and oxygen and the known mean property maps also support the formation region of the anticyclonic eddy as being on the Chilean shelf. The water off northern Chile is of tropical origin carried by the Peru-Chile Undercurrent southward [e.g., *Hormazabal et al.*, 2013].

The 315 day (20 April 2011 to 29 February 2012) displacement of 14.5° from 71°W to 85.5°W results in a mean westward translation velocity of c = 5.5 cm s^{-1}. With the rotational speed U reaching 20 cm s^{-1} at depths between 50 and 400 m, (Figures 2b and 5) the anticyclonic eddy is nonlinear (U/c > 1), which allows it to maintain a coherent structure as it propagates. The rotational speed of 20 cm s^{-1} is higher than the 8 cm s^{-1} described for the mean eddies which is based on the assumption of zero velocity at 1000 m depth [*Chaigneau et al.*, 2011]. Near 1000 m depth temperature and salinity measurements resulted in an increase in temperature and decrease in salinity when the anticyclone passed the mooring. As there is an increase of salinity with depth near 1000 m related to the salinity minimum at about 700 m from the Antarctic Intermediate Water [e.g., *Tsuchiya and Talley*, 1998] the vertical displacement of isopycnals in an anticyclone at 1000 m depth should be related to decreasing salinity. Although there was no current meter near 1000 m, the depth temperature and salinity records indicate that the eddy extended deeper than 1000 m, hence a velocity reference at 1000 m depth leads to reduced rotational speed.

One of eight floats with oxygen sensors deployed in April 2011 at ~20°S east of 85°W with a parking depth of 1000 m and profiling every 10 days was trapped according to the SSHA images in the strong anticyclonic mode-water eddy from 12 July at 22.5°S, 75°W to 30 October 2011 at 21.5°S, 79°W (Figure 8a). The eddy moved about 430 km westward in this time period which leads to a velocity of 4.6 cm s^{-1}, a little slower

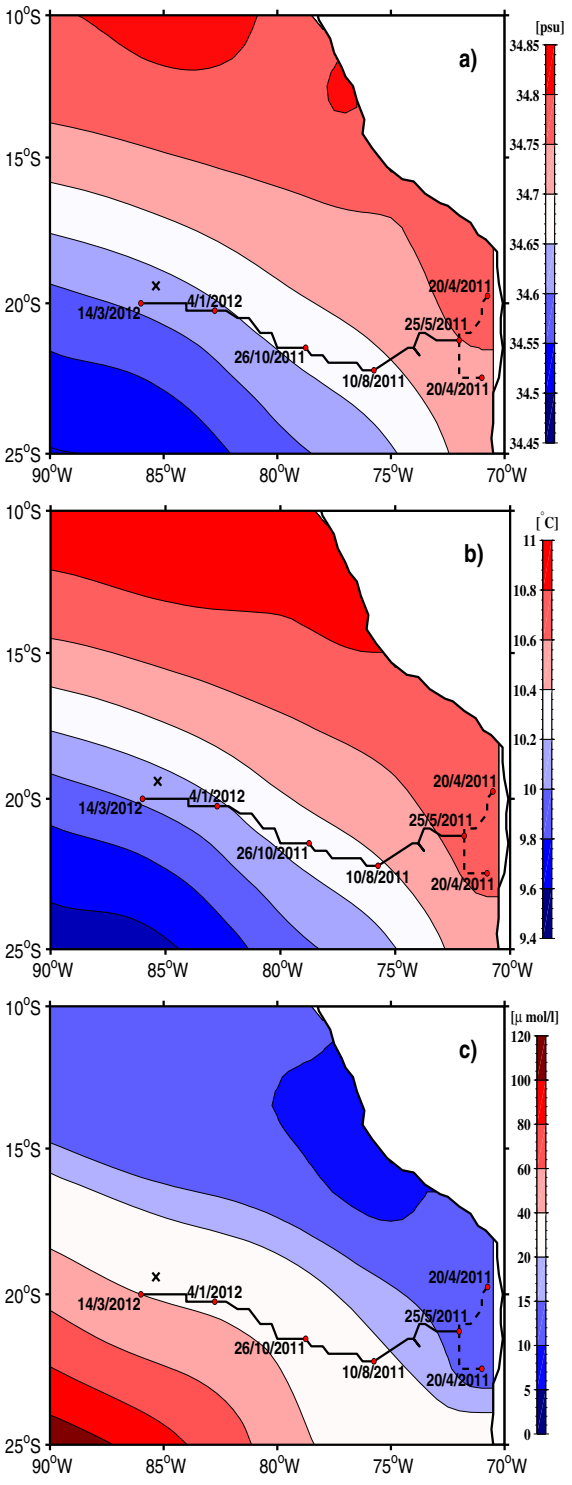

Figure 7. The path of the core of the anticyclonic eddy derived from SSHA maps from 20 April 2011 to 10 March 2012 (black line, some dates are marked) plotted on: (a) the mean salinity field, (b) the mean temperature field in °C, and (c) oxygen in µmol L^{-1} on the density surface $\sigma_\theta = 26.65$ kg m^{-3} (color) at about 330 m depth derived from the World Ocean Atlas 2009. The paths of two eddies near the shelf on 20 April 2011 that merged in May 2011 and are possibly the precursors of the strong anticyclone are shown by dashed lines.

than the 5.5 cm s^{-1} estimated from the SSHA field for the entire lifetime. In this period, the float data show enhanced geopotential anomalies in the layer 450 to 250 m depth (Figure 8b). When the float stayed in the eddy, the density at 400 m decreased by about 0.1 kg m^{-3} while the salinity and temperature at 400 m increased by about 1°C and 0.1. Due to a float programming error the lowest oxygen concentrations could not be recorded completely, therefore the oxygen distribution has to be presented at 475 m depth (Figure 8f) where the oxygen decreases by more than 20 µmol L^{-1}. The extremes for density, salinity, temperature, and oxygen at the Stratus mooring (Figure 4) were slightly higher, as the float was primarily located north of the eddy center and probably did not reach the core of the anticyclonic mode-water eddy, although the eddy core crossed to south of the mooring.

4. Discussion and Conclusion

At the northern boundary of the South Pacific subtropical gyre below the saline, warm and nutrient poor South Pacific Eastern Subtropical Surface Water (STSW), South Pacific Eastern Subtropical Mode Water (SPESMW) is located above the salinity minimum of the Antarctic Intermediate Water (AAIW) [*Fiedler and Talley*, 2006]. As SPESMW is formed in the southern subtropical gyre it has relatively low temperatures, low salinity, and high oxygen. The Peru Chile Undercurrent (PCUC) transports Equatorial Subsurface Waters (ESSW) southward, which is characterized by a subsurface salinity maximum, relatively warm subsurface waters, low oxygen concentrations, and high nutrient concentrations. Mode water or (intrathermocline eddies) formed off Chile are represented by subsurface lenses of saline, oxygen-deficient waters which are linked to the ESSW [*Hormazabal et al.*, 2013]. Our investigation shows that the strong water mass anomaly observed at the Stratus ORS in the eastern South Pacific in February/March 2012 was carried by an anticyclonic eddy. The density distribution reveals that it is a mode-water eddy with a thick lens of water that deepens the main thermocline. From SSHA satellite data and

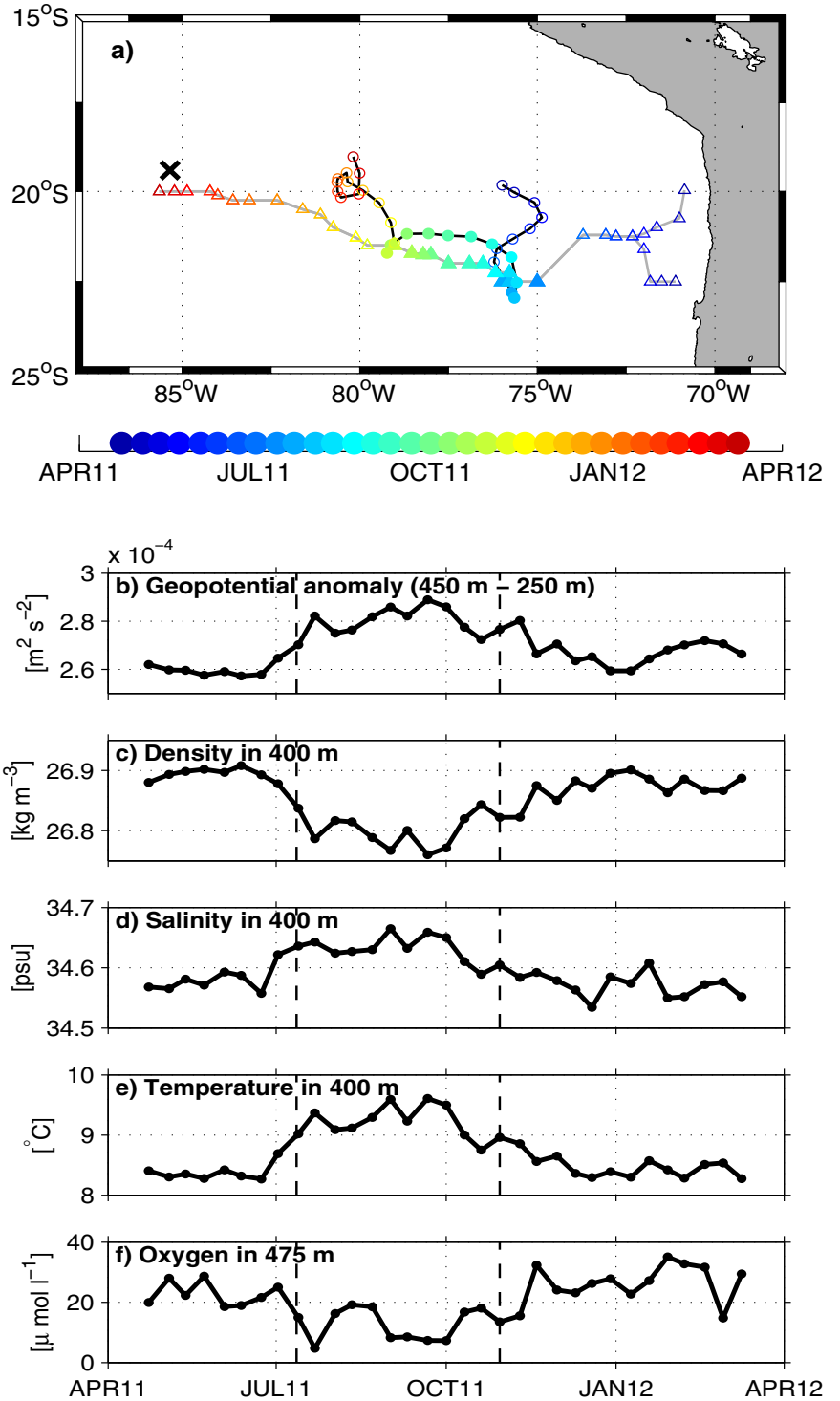

Figure 8. Observations from Argo floats showing: (a) float paths (circles) and the eddy path (triangles) color coded by time with symbols color filled at the time when the float was in the anticyclonic mode-water eddy; the Stratus mooring location is shown by an X, and time series of: (b) geopotential anomaly for the layer 450 to 250 m depth), (c) density at 400 m depth, (d) salinity at 400 m depth, (e) temperature at 400 m depth, and (f) oxygen at 475 m depth from a profiling float deployed on 2 April 2011 at 19.78°S, 76.49°W. Vertical dashed lines mark the period when the float was in the anticyclonic mode-water eddy, from 12 July 2011 at 22.5°S, 75°W to 30 October 2011 at 21.5°S, 79°W.

the temperature and salinity values on density surfaces it could be determined that the eddy originated about 11 months earlier off the Chilean coast, probably at 22.5°S, 71°W. An eddy formed at 19.75°S, 70.75°W merged in May 2011 with the eddy formed at 22.5°S, 71°W making the exact formation location of

Table 2. Comparisons of Properties and Anomalies of Mean Anticyclonic Eddies Between the Mode-Water Eddy at the Stratus Mooring in February/March 2012, Two Eddies at About 16°45′S in November 2012 Relative to Profiles Close to the Eddy [*Stramma et al*., 2013], and the Mean Values for 10°S to 30°S Relative to a Mean Climatology [*Chaigneau et al*., 2011][a]

	~20°S Stratus	~16°45′S *Stramma et al.* [2013] and *Chaigneau et al.* [2011]		
	Feb–Mar 2012	Open Ocean	Near-Shelf	Eastern Pacific
Vertical extent (m)	45–600	0–600	0–600	0–540
Radius (km)	38	48.8	52	57.6
Volume ($\times 10^{12}$ m^3)	2.5	4.7	5.2	5.5
AHA ($\times 10^{18}$ J)	5.8	3.7	17.7	8.7
ASA ($\times 10^{10}$ kg)	19.3	18.7	36.6	23.8
AOA ($\times 10^{16}$ μmol)	−10.5	−7.6	−10.0	

[a]Availably heat anomaly (AHA) and available salt anomaly (ASA) within one eddy are computed following *Chaigneau et al*. [2011] however relative to profiles close to the eddy instead of the mean climatology, and the same method was used to compute the available oxygen anomaly (AOA).

the strong anticyclone ambiguous. The higher temperature and salinity and the low oxygen probably identify ESSW being transported by the mode-water eddy.

Eddies generated south of 15°S have a mean lifetime of 50–60 days with about 3 out of 1000 eddies having a lifespan of 10 months [*Chaigneau et al*., 2008, Figure 5a]. Anticyclonic eddies move northwestward with a latitude displacement of 1.5° in 180 days [*Chaigneau et al*., 2008]. The coastal eddy at 22.5°S with a northward shift of 2.5° in 11 months would better match the typical northward displacement of anticyclonic eddies than the coastal eddy starting at 19.75°S with a slight mean southward shift on its way to the Stratus location. Examining all satellite sea surface temperature (SST) records along the eddy track, no significant temperature signature was found to further aid tracking. An earlier examination of surface drifter and Argo floats showed small SST signatures, for anticyclonic eddies, +0.2°C, and for cyclonic eddies, −0.2°C [*Holte et al*. 2013]; hence, it is not surprising that the eddy could not be followed in SST data.

The 315 day displacement of 14.5° from 71°W to 85.5°W results in a mean westward velocity of 5.5 cm s^{-1} and fits the typical westward propagation of 3–6 cm s^{-1} in the eastern South Pacific [*Chaigneau et al*., 2008] which is close to about 5 cm s^{-1} at 20°S [*Chaigneau and Pizarro*, 2005, Figure 3]. The anticyclonic velocity signature is seen in all current meter instruments between 13 and 601 m depth, while the oxygen drops to near zero for all oxygen records between 145 and 450 m depth. The maximum swirl velocity (meridional velocity component) reach more than 20 cm s^{-1} (Figure 4) and hence is much stronger than the described mean meridional velocity of up to 8 cm s^{-1}, which was derived with the assumption of zero velocity at 1000 m depth for the geostrophic component [*Chaigneau et al*., 2011, Figure 5].

For the mean anticyclonic eddies between 10°S and 30°S *Chaigneau et al*. [2011] computed the available heat anomalies (AHA) and available salt anomalies (ASA) relative to a climatological mean. *Stramma et al*. [2013] used the same method but relative to profiles located outside the eddy to compute AHA and ASA for the eddies observed in November 2012 in the open ocean and near the shelf off Peru at about 16°45′S. Using the same method [*Chaigneau et al*., 2011] the AHA, ASA and the available oxygen anomaly (AOA) for the eddy observed in February/March 2012 at the Stratus ORS were computed relative to the mean profiles on 9 February and 24 March 2012. For comparison also the AOA was computed for the two anticyclonic eddies in November 2012 at about 16°45′S (Table 2). As the estimated mean westward velocity of 5.5 cm s^{-1} is high compared to the westward velocity measured in 2012 at the Stratus mooring, the lower mean westward velocity of 4 cm s^{-1} measured at 20 m depth in February and March 2012 at the Stratus ORS is used to convert the time axis to a space axis for the period 9 February to 24 March 2012, which leads to a total extent of the outer eddy boundaries of 148 km. As oxygen data were measured only below 45 m, the anomalies were computed only for 45–600 m depth. Although the estimated radius of the core of the eddy and the volume is smaller than the ones described in the literature, AHA and ASA are of similar size as the mean eastern Pacific and the open ocean eddy in November 2012. The AOA of -10.5×10^{16} μmol is slightly larger than the AOA computed here for the two eddies along 16°45′S. The expected reason is that at the Stratus ORS the climatological mean oxygen distribution is high, and therefore the low oxygen content in the eddy leads to a larger anomaly than in regions where the mean local oxygen value is low. As the eddy core passes to the south of the Stratus ORS and because a lower translation speed than the estimated mean westward speed was used in the computation, the estimated eddy diameter, available heat, salt, and

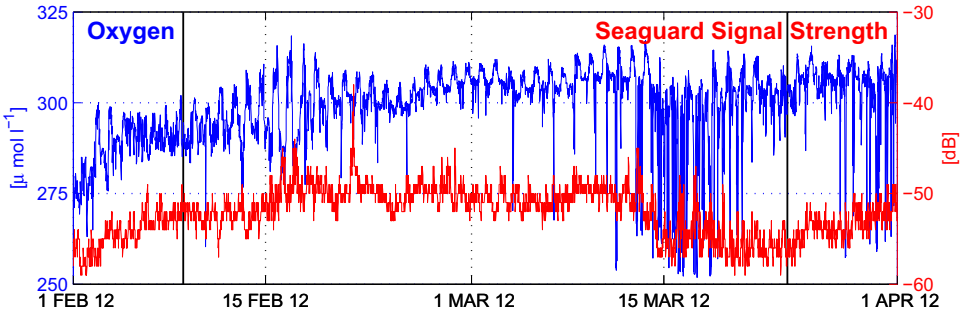

Figure 9. The unfiltered oxygen and Seaguard acoustic signal strength time series at 45 m depth for the period of the mode-water eddy passage from 1 February to 1 April 2012. The dates for the eddy passage are marked by vertical black lines on 9 February 2012 and 24 March 2012.

oxygen anomalies probably underestimate the anomalies. Nevertheless, it is of interest to attempt to quantify the available anomaly in the eddy.

The observed changes of 2°C in temperature and 0.2 in salinity at 401 m depth (Figure 3) are about twice as large as the described mean differences [*Chaigneau et al*., 2011, Figure 5] and should be related to the strong differences in temperature and salinity between the formation region and the eventual location at ~85.5°W. The fact that the eddy maintained the original temperature and salinity values indicated that the water trapped in the eddy stayed isolated from the surrounding water masses. The high U/c ratio of this eddy shows that there is trapped fluid within the eddy interior and that water from the Chilean shelf region is carried into the open ocean to the Stratus site. The low oxygen observed at the Stratus mooring could be either water from the formation region near the shelf or locally reduced in the mode-water eddy. The isolated water mass and the shoaling of the seasonal pycnocline by this anticyclonic mode-water eddy could lead to high productivity and oversaturated oxygen in the near surface layer and a reduction to almost zero oxygen in the subsurface layer of the anticyclonic eddy by the remineralization of organic material by bacteria and zooplankton during the 11 month travel time leading to the extremely low oxygen values between 145 and 450 m depth.

The increase of oxygen at 45 m depth at the time when the anticyclone passed by might be related to the mode-water type structure of the anticyclone. The uplift of the near surface isopycnals upwells a significant fraction of the nutrients required to sustain primary production to the near surface layer and generates extraordinary diatom blooms with highest chlorophyll values in the upper ocean while remineralization of the biomass in the thermocline strongly reduces the oxygen level [*McGillicuddy et al*., 2007]. At the surface no chlorophyll signals could be determined in chlorophyll satellite data; however, the chlorophyll a signal is expected at the base of the surface mixed layer [*McGillicuddy et al*., 2007].

No chlorophyll or biological measurements were made on Stratus 11; however, there is indirect evidence for enhanced primary production. The temperature records in the upper 35 m show the late summer warming from January to March 2012 (Figure 4a). Below the warming surface layer the temperatures at 46.5 and 62.5 m decrease from 10 February to early March 2012 by 0.9 and 0.3°C, respectively, due to the uplift of the mode-water anticyclone. Although the upper 35 m is warming and as a result the stronger vertical density gradient should oppose downward mixing of oxygen from the surface, the oxygen increases beginning in early February 2012. At that time the oxygen saturation exceeds 100%, most likely due to intense oxygen production by a diatom bloom. The extremely low oxygen in the layer 145–450 m might be caused by oxygen consumption due to remineralization of the sinking biomass in the isolated water body of the anticyclone.

The acoustic backscatter signal strength from the acoustic current meter at 45 m (Figure 9) indicates high zooplankton abundance from mid-February to mid-March 2012. The signal strength increases from early February to mid-March, which might be related to enhanced zooplankton abundance [e.g., *Heywood et al*., 1991], although some enhanced biomass of highly migratory pelagic fish can be carried by mode-water eddies [*Hormazabal et al*., 2013]. The indicated zooplankton appearance in the backscatter signal strength takes place at the same time as the chlorophyll increase as indicated by the oxygen increase without a

lagged delay. In the Atlantic a lag for the passage of two eddies was described for the Bermuda Testbed Mooring, however, the lags were only 0 and 2 days [*Jiang et al*., 2007]. The unfiltered oxygen record shows a diurnal cycle with lower oxygen at night when no photosynthesis takes place. At night the backscatter signal strength increases showing the diurnal migration of the zooplankton. In mid-February and mid-March 2012 the oxygen records show higher diurnal variability (Figure 9) probably caused by mixing within the strong northward velocity components of the eddy swirl velocity with enhanced turbulence at these two time periods. There was also a temperature increase below 35 m depth (Figure 4a) in mid-February and mid-March 2012, as at this depth the cores of the mode-water eddy as well as of the cyclonic eddy in late March 2012 have lower temperatures, while the outer regions of the eddies show normal, relatively higher temperatures. Certainly the mode-water eddy started with low oxygen when it was formed off Chile. No data are available to show enhanced primary production when the eddy moved westward. At the Stratus ORS there are indications of enhanced primary production, hence we expect that the eddy was formed with a low-oxygen load, which was maintained at a low oxygen level due to primary production as expected for mode-water anticyclones.

The SSHA maximum in October to December 2011 (Figure 3) was related to an anticyclonic eddy and the minimum in April 2012 to a strong cyclonic eddy (Figure 6). Despite the large SSHA, the swirl velocity of the eddy in late 2011 was only larger than 10 cm s^{-1} in the upper 200 m and less than 15 cm s^{-1} below 300 m in late March and April 2012. The related geostrophic sea surface swirl velocity derived from the SSHA satellite data is weaker than the subsurface swirl velocity (Figure 5). These eddies with strong SSHA signals had weak water mass anomalies, while the strong mode-water anticyclone only had a weak SSHA signature but strong subsurface swirl velocities and water mass anomalies. Therefore, SSHA alone is not sufficient to specify the eddy strength and in situ measurements are needed.

Essentially all of the observed mesoscale features outside of the tropical band 20°S–20°N are nonlinear by the U/c metric and imply that there is trapped fluid within the eddy interior [*Chelton et al*., 2011b]. As eastern Pacific eddies do not return back to the coastal regions, the anomalous water mass and biogeochemical parameters will mix with the surrounding water and modify the open ocean water properties. Thus, these eddies do play a role in setting properties and in bringing nutrients to the Stratus site.

To better understand the influence of eddies on the eastern tropical South Pacific a detailed interdisciplinary survey of an eddy [e.g., *Benitez-Nelson et al*., 2007] by biological and chemical measurements from a ship survey when combined with mooring observations should lead to a better understanding on biological, chemical, and physical processes involved. As the SSHA signal is weak before the eddy falls apart, it would be good to make measurements of a dissipating eddy, which probably points to the use of autonomous instruments like gliders. There is a fundamental challenge for a single point mooring in observing eddy structures, that of not knowing exactly how the eddy tracks past the mooring, in other words not knowing what slice of the eddy structure is obtained at what radius from the eddy center. The high vertical and temporal resolution of the single surface mooring needs complementary spatial sampling. In the VOCALS Regional Experiment, *Holte et al*. [2013] obtained comprehensive synoptic surveys of eddies with an underway CTD and shipboard ADCP. However, in the future, based on these more recent findings, we see that more comprehensive oxygen and nutrient sampling would have value and should be included in such investigations. This would support efforts to better understand the role of eddies in the offshore transport of oxygen poor and nutrient rich coastal water in comparison to the possibility of vertical mixing bringing up SPESMW from below.

Appendix A: Mooring and Instrument Details

The Stratus mooring is called the Stratus Ocean Reference Station (ORS) and is typically serviced once a year. The Stratus ORS is a surface mooring with a 3 m diameter buoy that carries meteorological systems. The Stratus ORS is supported by the United States National Oceanic and Atmospheric (NOAA) Climate Observation Program. Initially, in the early years of the mooring deployment, there was limited instrumentation on the mooring line to the upper 300 m; it was not equipped until recently to observe eddies and their vertical structure. Later, however, in recognition of the dominance of the eddy variability, where velocities can exceed 60 cm s^{-1} in contrast with mean flows of only several cm s^{-1}, and of the fresh mode water below the surface layer, deeper sensors were added to better observe the eddies and resolve the vertical

structure. Most recently, collaboration between the authors of this paper and interest in the OMZ has lead to the addition of Aanderaa Seaguard current meters with optodes and also stand alone optodes. The surface mooring uses chain and wire rope in the upper 2000 m of the mooring; and the instrument array in the upper part of the mooring is always close to vertical.

Ten oxygen sensors were deployed to observe the oxygen field in the upper ocean. The seven optodes moored below 200 m depth recorded the entire deployment period while the instruments at 45, 87.3, and 145 m failed either in January or April 2012. The optodes on the Aanderaa Seaguard deployed by WHOI were not independently calibrated; the manufacturer's calibrations were used. The oxygen loggers deployed by GEOMAR at 322 and 353 m depth were calibrated by the manufacturer and further refined by a calibration made in the Atlantic Ocean on cruises which took place prior to the deployment in the Pacific Ocean Stratus mooring. Three Aanderaa RCM 11 current meters were deployed at 13, 20, and 32.5 m. VMCMs (Vector Measuring Current Meters) were also deployed as indicated in Table 1.

The RCM current meters agree well with the VMCMs, as long as the VMCM propeller sensors are not fouled by fishing line. An RDI Workhorse 300 kHz profiler was deployed at 135 m depth looking upward with 10 m bins. This instrument stopped working prematurely on 30 December 2011. Current meters, both those measuring a single point and the profilers, have the function of their compasses verified by rotation through 360° and comparison to a reference compass. A magnetic deviation of 7.1792° has been applied to all currents. All SeaBird temperature/conductivity instruments mounted on the mooring are sent to SeaBird before and after the deployment for calibration. Temperature recorders are calibrated in a temperature bath at WHOI.

The new Stratus ORS mooring is deployed before the old mooring is recovered to obtain several days of overlapping records, which aids in identifying any drifts or offsets that have developed in the instrumentation that has been deployed for a year. Shipboard CTD profiles are also taken close to the mooring. Upon recovery, timing marks are inserted on the data records on instruments measuring temperature by immersing instruments in ice baths. These timing marks, together with start and stop times were used to verify instrument clocks and adjust the base of the records if needed. Pre and postcalibrations were used together with instrument intercomparisons to identify and resolve biases and drifts in temperature and salinity. Intercomparisons were used to check the quality of the velocity data. When mechanical current meters were fouled by fishing line or degraded by biofouling, the records were truncated. Noisy velocity data from acoustic profilers were rejected.

Acknowledgments

Financial support was received through Woods Hole Oceanographic Institution (R.A.W. and S.B.) and the GEOMAR (L.S. and R.C). The Stratus Ocean Reference Station is supported by the National Oceanic and Atmospheric Administration's (NOAA) Climate Observation Program (NA09OAR4320129). This work is a contribution of the DFG-supported project SFB754 (http://www.sfb754.de) which is supported by the Deutsche Forschungsgemeinschaft. The altimeter products were produced by Ssalto/Duacs and distributed by Aviso with support from CNES.

References

Benitez-Nelson, C. R., et al. (2007), Mesoscale eddies drive increased silica export in the subtropical Pacific Ocean, *Science*, *316*, 1017–1021, doi:10.1126/science.1136221.

Bertrand, A., A. Chaigneau, S. Peraltilla, J. Ledesma, M. Graco, F. Monetti, and F. Chavez (2011), Oxygen: A fundamental property regulating pelagic ecosystem structure in the coastal Southeastern tropical Pacific, *PLoS ONE*, *6*(12), e29558, doi:10.1371/journal.pone.0029558.

Bopp, L., C. Le Quere, M. Heimann, A. C. Manning, and P. Monfray (2002), Climate induced oceanic oxygen fluxes: Implications for the contemporary carbon budget, *Global Biogeochem. Cycles*, *16*(2), 1022, doi:10.1029/2001GB001445.

Boyer, T. P., J. I. Antonov, O. K. Baranova, H. E. Garcia, D. R. Johnson, R. A. Locarnini, A. V. Mishonov, D. Seidov, I. V. Smolyar, and M. M. Zweng (2009), Introduction, in *World Ocean Database 2009, NOAA Atlas NESDIS 66*, edited by S. Levitus, chap. 1, 216 pp., U.S. Gov. Print. Off., Washington, D. C.

Chaigneau, A., and O. Pizarro (2005), Eddy characteristics in the eastern South Pacific, *J. Geophys. Res.*, *110*, C06005, doi:10.1029/2004JC002815.

Chaigneau, A., A. Gizolme, and C. Grados (2008), Mesoscale eddies off Peru in altimeter records: Identification algorithms and eddy spatio-temporal patterns, *Prog. Oceanogr.*, *79*, 106–119.

Chaigneau, A., M. Le Texier, G. Eldin, C. Grados, and O. Pizarro (2011), Vertical structure of mesoscale eddies in the eastern South Pacific Ocean: A composite analysis from altimetry and Argo profiling floats, *J. Geophys. Res.*, *116*, C11025, doi:10.1029/2011JC007134.

Chelton, D. B., M. G. Schlax, R. M. Samelson, and R. A. de Szoeke (2007), Global observations of large oceanic eddies, *Geophys. Res. Lett.*, *34*, L15606, doi:10.1029/2007GL030812.

Chelton, D. B., P. Gaube, M. G. Schlax, J. J. Early, and R. M. Samelson (2011a), The influence of nonlinear mesoscale eddies on near-surface oceanic chlorophyll, *Science*, *334*, 328–332.

Chelton, D. B., M. G. Schlax, and R. M. Samelson (2011b), Global observations of nonlinear mesoscale eddies, *Prog. Oceanogr.*, *91*, 167–216.

Colas, F., J. C. McWillliams, X. Capet, and J. Kurian (2012), Heat balance and eddies in the Peru-Chile current system, *Clim. Dyn.*, *39*, 509–529, doi:10.1007/s00382-011-1170-6.

Colas, F., X. Capet, J. C. McWilliams, and Z. Li (2013), Mesoscale eddy buoyancy flux and eddy-induced circulation in eastern boundary currents, *J. Phys. Oceanogr.*, *43*, 1073–1095, doi:10.1175/JPO-D-11-0241.1.

Colbo, K., and R. Weller (2007), The variability and heat budget of the upper ocean under the Chile-Peru stratus, *J. Mar. Res.*, *65*, 607–637.

Colbo, K., and R. Weller (2009), Accuracy of the IMET sensor package in the subtropics, *J. Atmos. Oceanic Technol.*, *26*, 1867–1890, doi:10.1175/2009JTECHO667.1.

Czeschel, R., L. Stramma, F. U. Schwarzkopf, B. S. Giese, A. Funk, and J. Karstensen (2011), Middepth circulation of the eastern tropical South Pacific and its link to the oxygen minimum zone, *J. Geophys. Res.*, *116*, C01015, doi:10.1029/2010JC006565.
Dewar, W. K., G. R. Flierl (1987), Some effects of the wind on rings, *J. Phys. Oceanogr.*, *17*, 1653–1667.
Dickey, T. D., F. Nencioli, V. S. Kuwahara, C. Leonard, W. Black, Y. M. Rii, R. R. Bidigare, and Q. Zhang (2008), Physical and bio-optical observations of oceanic cyclones west of the island of Hawai'i, *Deep Sea Res., Part II*, *55*, 1195–1217.
Fiedler, P. C., and L. D. Talley (2006), Hydrography of the eastern tropical Pacific: A review, *Prog. Oceanogr.*, *69*, 143–180.
Flierl, G. R. (1981), Particle motions in large-amplitude wave fields, *Geophys. Astrophys. Fluid Dyn.*, *18*, 39–74.
Gruber, N., Z. Lachkar, H. Frenzel, P. Marchesiello, M. Münnich, J. C. McWilliams, T. Nagai, and G.-K. Plattner (2011), Eddy-induced reduction of biological production in eastern boundary upwelling systems, *Nat. Geosci.*, *4*, 787–792, doi:10.1038/NGEO1273.
Haury, L. R. (1984), An offshore eddy in the California Current system. Part VI: Plankton distributions, *Prog. Oceanogr.*, *13*, 95–111.
Heywood, K. J., S. Scrope-Howe, and E. D. Barton (1991), Estimation of zooplankton abundance for shipborne ADCP backscatter, *Deep Sea Res., Part A*, *38*, 677–691.
Holte, J., F. Straneo, C. Moffat, R. Weller, and J. T. Farrar (2013), Structure and surface properties of eddies in the southeast Pacific Ocean, *J. Geophys. Res.*, *118*, 1–15, doi:10.1002/jgrc.20175.
Hormazabal, S., V. Combes, C. E. Morales, M. A. Correa-Ramirez, E. Di Lorenzo, and S. Nunez (2013), Intrathermocline eddies in the coastal transition zone off central Chile (31–41°S), *J. Geophys. Res.*, *118*, 4811–4821, doi:10.1002/jgrc.20337.
Jiang, S. W., T. D. Dickey, D. K. Steinberg, and L. P. Madin (2007), Temporal variability of zooplankton biomass from ADCP backscatter time series data at the Bermuda Testbed Mooring site, *Deep Sea Res., Part I*, *54*, 608–636.
Johnson, G. C., and K. E. McTaggart (2010), Equatorial Pacific 13°C water eddies in the eastern subtropical South Pacific Ocean, *J. Phys. Oceanogr.*, *40*, 226–236, doi:10.1175/2009JPO4287.1.
Karstensen, J., L. Stramma, and M. Visbeck (2008), Oxygen minimum zones in the eastern tropical Atlantic and Pacific oceans, *Prog. Oceanogr.*, *77*, 331–350.
Kessler, W. S. (2006), The circulation of the eastern tropical Pacific: A review, *Prog. Oceanogr.*, *69*, 181–217.
Koblinsky, C. J., J. J. Simpson, and T. D. Dickey (1984), An offshore eddy in the California Current system. Part II: Surface manifestation, *Prog. Oceanogr.*, *13*, 51–69.
Ledwell, J. R., D. J. McGillicuddy Jr., and L. A. Anderson (2008), Nutrient flux into an intense deep chlorophyll layer in a mode-water eddy, *Deep Sea Res., Part II*, *55*, 1139–1160.
Lukas, R., and F. Santiago-Mandujano (2001), Extreme water mass anomaly observed in the Hawaii Ocean Time-series, *Geophys. Res. Lett.*, *28*, 2931–2934.
Matear, R. J. and C. Hirst (2003), Long-term changes in dissolved oxygen concentrations in the ocean caused by protracted global warming, *Global Biogeochem. Cycles*, *17*, 1125, doi:10.1029/2002GB001997.
McCartney, M. S. (1982), The subtropical recirculation of Mode Water, *J. Mar. Res.*, *40*, supplement, 427–464.
McGillicuddy, D. J., Jr., et al. (2007), Eddy/wind interactions stimulate extraordinary mid-ocean plankton blooms, *Science*, *316*, 1021–1026.
Mechoso, C. R., et al. (2014), Ocean-cloud-atmosphere-land interactions in the Southeastern Pacific: The VOCALS Program, *Bull. Am. Meteorol. Soc.*, doi:10.1175/BAMS-D-11-00246.1, in press.
Morales, C. E., S. Hormazabal, M. Correa-Ramirez, O. Pizarro, N. Silva, C. Fermandez, V. Anabalon, and M. L., Torreblanca (2012), Mesoscale variability and nutrient-phytoplankton distributions off central-southern Chile during the upwelling season: The influence of mesoscale eddies, *Prog. Oceanogr.*, *104*, 17–29, doi:10.1016/j.pocean.2012.04.015.
Paulmier, A., and D. Ruiz-Pino (2009), Oxygen minimum zones (OMZs) in the modern ocean, *Prog. Oceanogr.*, *80*, 113–128, doi:10.1016/j.pocean.2008.08.001.
Paulmier, A., D. Ruiz-Pino, V. Garcon, and L. Farias (2006), Maintaining of the eastern South Pacific oxygen minimum zone (OMZ) off Chile, *Geophys. Res. Lett.*, *33*, L20601, doi:10.1029/2006GL026801.
Simpson, J. J. (1984), An offshore eddy in the California Current system. Part III: Chemical Structure, *Prog. Oceanogr.*, *13*, 71–93.
Simpson, J. J., T. D. Dickey, and C. J. Koblinsky (1984), An offshore eddy in the California Current system. Part I: Interior dynamics, *Prog. Oceanogr.*, *13*, 5–49.
Stramma, L., G. C. Johnson, J. Sprintall, and V. Mohrholz (2008), Expanding oxygen-minimum zones in the tropical oceans, *Science*, *320*, 655–658.
Stramma, L., G. C. Johnson, E. Firing, and S. Schmidtko (2010a), Eastern Pacific oxygen minimum zones: Supply paths and multidecadal changes, *J. Geophys. Res.*, *115*, C09011, doi:10.1029/2009JC005976.
Stramma, L., S. Schmidtko, L. A. Levin, and G. C. Johnson (2010b), Ocean oxygen minima expansions and their biological impacts, *Deep Sea Res., Part I*, *57*, 587–595.
Stramma, L., H. W. Bange, R. Czeschel, A. Lorenzo, and M. Frank (2013), On the role of mesoscale eddies for the biological productivity and biogeochemistry in the eastern tropical Pacific off Peru, *Biogeosciences*, *10*, 7293–7306, doi:10.5194/bg-10-7293-2013.
Tsuchiya, M. and L. D. Talley (1998), A Pacific hydrographic section at 88°W: Water-property distribution, *J. Geophys. Res.*, *103*, 12,899–12,918, doi:10.1029/97JC03415.
Yang, M., et al. (2011), Atmospheric sulfur cycling in the southeastern Pacific—Longitudinal distribution, vertical profile, and diel variability observed during VOCALS-REx, *Atmos. Chem. Phys.*, *11*, 5079–5097, doi:10.5194/acp-11-5079-2011.